Available online at www.sciencedirect.com
SCIENCE DIRECT®
Journal of Nuclear Materials 341 (2005) 97–102
journal of nuclear materials
www.elsevier.com/locate/jnucmat

Effect of heat treatment on the microstructure and corrosion resistance of a Zr–Sn–Nb–Fe–Cr alloy

Wenqing Liu *, Qiang Li, Bangxin Zhou, Qingsong Yan, Meiyi Yao

Instrumental analysis and research center, Shanghai University, P.O. Box 129, Shanghai, 200444, People's Republic of China

Received 3 August 2004; accepted 17 January 2005

Abstract

Zr–Sn–Nb–Fe–Cr zirconium alloy specimens treated in different ways were exposed to 0.01 M LiOH aqueous solution at 350 °C, 16.8 MPa. The microstructures of these specimens were investigated by transmission electron microscopy (TEM). It is found that the specimen treated by 800 °C/500 °C had best corrosion resistance among all the specimens. TEM analysis of this specimen showed that, in addition to $Zr(Fe,Cr)_2$, there existed Zr–Nb–Fe type precipitates containing much more Nb element, which reduced niobium content in αZr solid solution and, therefore, resulted in an improvement in the corrosion resistance of Zr–Sn–Nb–Fe–Cr zirconium alloy.

1. Introduction

Zircaloy has been successfully used as fuel cladding in nuclear reactor environments for many years. However, as light water reactors tend to be operated in more severe environments, that is, increased burn-up, high operation temperature, and high pH in first loop, higher corrosion resistant alloys have been continuously developed as a substitute for Zircaloy. Some achievements were made by modifying the chemical composition of Zircaloy.

Several new Nb-containing zirconium alloys such as ZIRLO (Zr–1.0Nb–1.0Sn–0.1Fe) [1], M5 (Zr–1Nb–O) [2], E635 (Zr–1.0Nb–1.0Sn–0.4Fe) [3] and N18 (Zr–0.3Nb–1.0Sn–0.3Fe–0.1Cr) [4] were developed and are being tested in-reactor. However, it is reported that the corrosion behavior of Nb-containing Zr alloy is very sensitive to the microstructures that could be changed by heat treatment. Therefore, it is necessary to establish an appropriate thermal process for the optimum corrosion resistance of alloys containing Nb.

Thorvaldsson et al. [5] proposed that the corrosion resistance of Zircaloy-4 can be related to the accumulated annealing parameter ($\sum A$), which is an index of the total amount of heat treatment received in α-region after the β-quenching. The parameter combines the annealing time (t) in hours and temperature (T) in Kelvin of each heat treatment. The accumulated annealing parameter ($\sum A$) can be described as follows:

$$\sum A = \sum_i t_i \exp[-Q/RT_i],$$

where Q is the activation energy and R is the gas constant. The weight gain of Zircaloy-4 decreased with increasing accumulated annealing parameter [6,7]. But Zhou et al. [8] proposed that the solid solution content

* Corresponding author. Tel.: +86 21 66135032; fax: +86 21 66135005.
E-mail address: wqliu@staff.shu.edu.cn (W. Liu).

0022-3115/$ - see front matter © 2005 Elsevier B.V. All rights reserved.
doi:10.1016/j.jnucmat.2005.01.007

of Fe and Cr in αZr resulted from different heat treatments was an essential factor affecting the corrosion behavior of Zircaloy-4.

Baek et al. [9] and Isobe et al. [10] studied the corrosion resistance of Nb-containing zirconium alloys in relation to accumulated annealing parameter, and found that weight gain increased with accumulated annealing parameter. This result is contrary to that of Zircaloy-4 in PWR.

Previous work by us [11,12] on Nb-containing zirconium alloys had revealed that a uniform distribution of fine βNb (containing iron) particles were important factors for improving the corrosion resistance. In this study, the corrosion resistance of Zr–Sn–Nb–Fe–Cr alloys containing 0.39% Nb in relation to heat treatment and microstructure was investigated.

2. Experimental procedures

2.1. Specimens

The vacuum consumable arc remelting method was employed for producing 5 kg ingot of Zr–Sn–Nb–Fe–Cr zirconium alloy. The chemical compositions of the alloys are shown in Table 1. β-Quenching treatment in water was conducted to homogenize the composition within the ingot after being hot forged. Then the ingot was made into plates of about 0.5 mm thickness through various rolling and intermediate annealing processes. The last cold rolling reduction was about 50%. The heat treatments before the final cold rolling were carried out at two different conditions, i.e., 680 °C for 5 h and 800 °C for 1 h. The final heat treatments were carried out at 500 °C for 30 h or 560 °C for 10 h. The above-mentioned heat treatment processes gave four kinds of specimens, denoted as 680 °C/500 °C, 680 °C/560 °C, 800 °C/500 °C and 800 °C/560 °C. The microstructure of heat-treated specimens was investigated by a transmission electron microscope (TEM) (JEM-2010F) equipped with energy dispersive spectroscopy (EDS). The TEM specimens were prepared by mechanical grinding (up to 60 μm) and twin-jet polishing in a solution of ethanol (80%) and perchloric acid (20%) at 25 °C (applied voltage and current = 20 V/30 mA). The composition analyses on the precipitates in the heat-treated specimens were conducted with EDS. More than 20 precipitates from each kind of foil specimen were analyzed to minimize the detection error.

2.2. Corrosion tests

Specimens for corrosion test were prepared after the final heat treatment. Rectangular specimens, $20 \times 25\ mm^2$ in size, were chemically polished using a pickling solution (a mixture of 10% HF, 30% HNO_3, 30% H_2SO_4 and 30% H_2O) in the final step. The out-pile corrosion test was conducted in 0.01 M LiOH aqueous solution at 350 °C under a pressure of 16.8 MPa and in 400 °C superheated steam under a pressure of 10.3 MPa. The corrosion resistance of the specimens was evaluated by measuring their weight gain per unit surface area in relation to the exposure time. The corro-

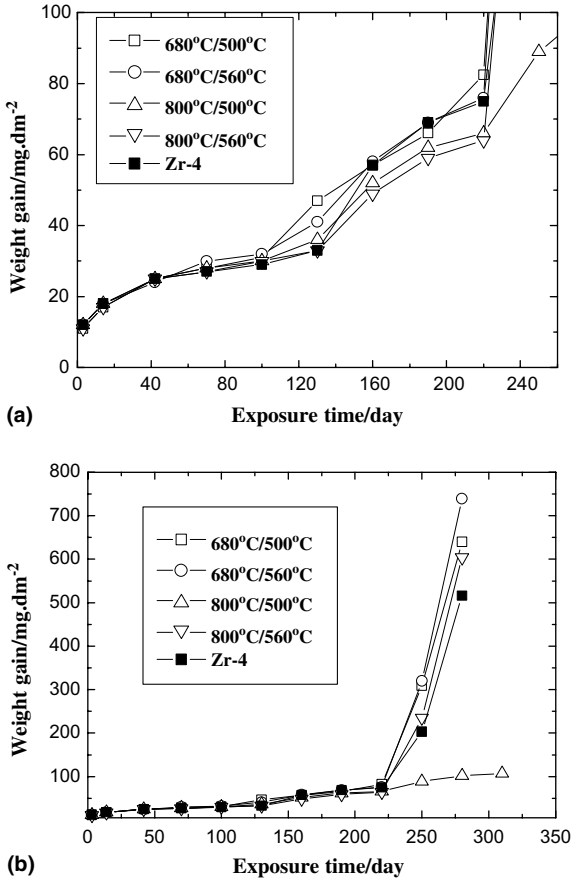

Fig. 1. Weight gain against exposed time of Zr–Sn–Nb–Fe–Cr specimens tested in M LiOH solution at 350 °C, (a) and (b) are plotted in different scale of weight gain.

Table 1
Chemical composition of Zr–Nb–Sn–Fe–Cr alloy and Zircaloy-4

Alloy	Sn (wt%)	Nb (wt%)	Fe (wt%)	Cr (wt%)	O (ppm)	Zr (wt%)
Zr–Nb–Sn–Fe–Cr alloy	1.0	0.39	0.31	0.05	480	Bal.
Zircaloy-4	1.2		0.21	0.10	500	Bal.

sion tests of Zircaloy-4 specimens, which have the chemical composition as shown in Table 1, were also conducted as reference.

3. Results and discussion

3.1. Effect of heat treatment on corrosion behavior

The effect of heat treatments on the corrosion behavior of Zr–Sn–Nb–Fe–Cr alloy specimens tested in different media is shown in Figs. 1 and 2. The corrosion resistance of 800 °C/500 °C specimens was remarkably superior to that of other three kinds of specimens and Zircaloy-4 specimens when corrosion tests were carried in 0.01 M LiOH aqueous solution (Fig. 1). The weight gain of four kinds of specimens in 400 °C superheated steam for 160 days increased with the order of 800 °C/560 °C, 680 °C/500 °C, 800 °C/500 °C and 680 °C/560 °C (Fig. 2). The accumulated annealing parameters of 680 °C/500 °C, 680 °C/560 °C, 800 °C/500 °C and 800 °C/560 °C specimens, Q/R of 34 000 K was obtained and used, were 2.363×10^{-15}, 2.381×10^{-15}, 1.808×10^{-14} and 1.810×10^{-14}, respectively. These results were different from that of other zirconium alloys containing Nb studied by Baek et al. [9] and Isobe et al. [10], which illustrated that the corrosion resistance had no certain relation to the accumulated annealing parameter. Therefore, the different corrosion behavior may be due to the microstructure difference of the specimens.

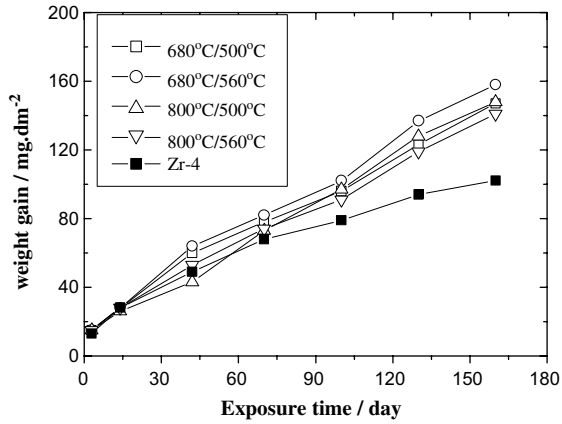

Fig. 2. Weight gain against exposed time of Zr–Sn–Nb–Fe–Cr specimens tested in 400 °C superheated steam.

3.2. Microstructure of heat-treated specimens

The microstructures of the four kinds of specimens were investigated by TEM/EDS analysis. It was observed

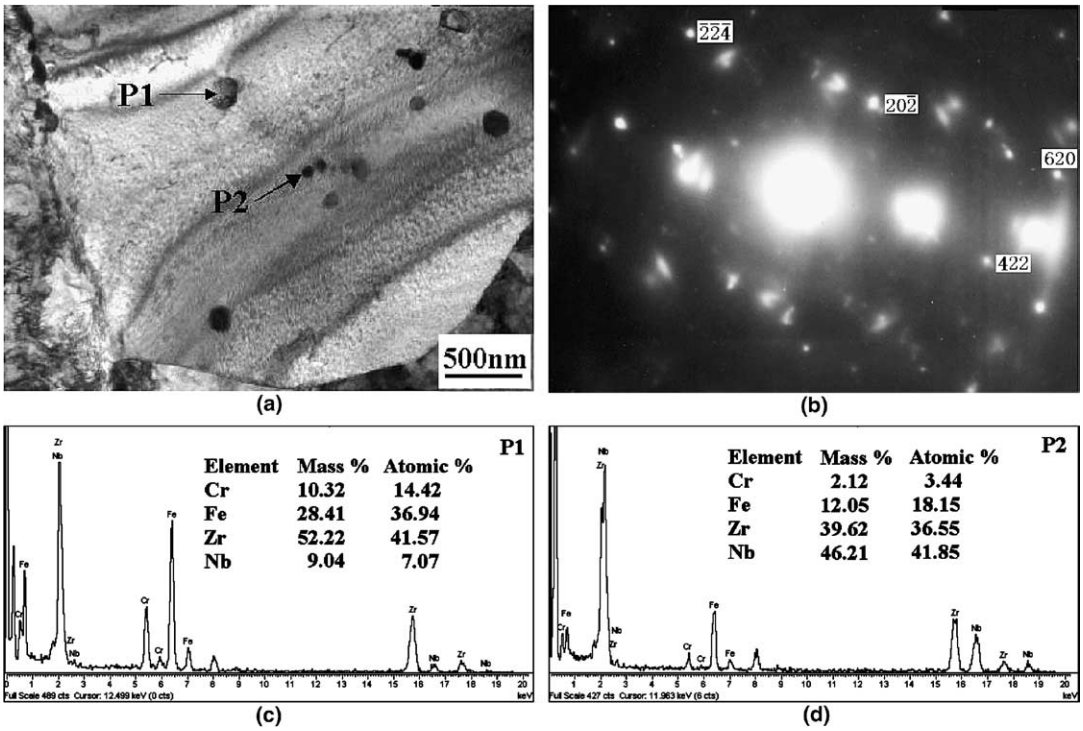

Fig. 3. TEM micrograph, SAD and EDS spectra for precipitates of Zr–Sn–Nb–Fe–Cr specimen treated by 800 °C/500 °C.

that there was no obvious difference on the size, shape and distribution of precipitates in these specimens (Figs. 3–6). There existed some unrecrystallized areas in the 800 °C/500 °C and 680 °C/500 °C specimens (Figs. 3 and 5). Since it was hard to recognize the precipitates in unrecrystallized areas, only the precipitates in recrystallized areas were analyzed with EDS. Due to a contribution of the surrounding Zr-matrix, the EDS analysis showed that the Zr content in the same kind precipitates is notably different, but there is only little deviation about Fe/Nb ratio of the same kind precipitates. The EDS analysis revealed that all the precipitates in these specimens contained niobium, which was consistent with that of zirconium alloys containing niobium to 0.4% studied by Isobe et al. [10] and Kim et al. [13]. This result indicated that the solubility limit of Nb in the matrix might be lower than 0.4%, although the maximum solubility limit of Nb in the matrix of Zr–Nb alloy is 0.6%.

Fig. 3(a) shows the precipitates in 800 °C/500 °C specimen. The bigger precipitate particle (P1) in the specimen was identified by the electron diffraction pattern (Fig. 3(b)) as cubic $Zr(Fe,Cr)_2$-type precipitate, which contains 7.07 at.% Nb by EDS analysis (Fig. 3(c)). However, the content of Nb in the small precipitate (P2) was 41.85 at.% (Fig. 3(d)), which is consistent with the result obtained by Mardon et al. [2] and Nikulina et al. [3], who identified this type precipitate as $Zr(Nb,Fe,Cr)_2$ having a hexagonal lattice with $a = 0.51$ nm and $c = 0.83$ nm. The EDS analysis revealed that there existed $Zr(Fe,Cr)_2$ type and Zr–Nb–Fe type, might be $Zr(Nb,Fe,Cr)_2$, intermetallic compounds in the specimens.

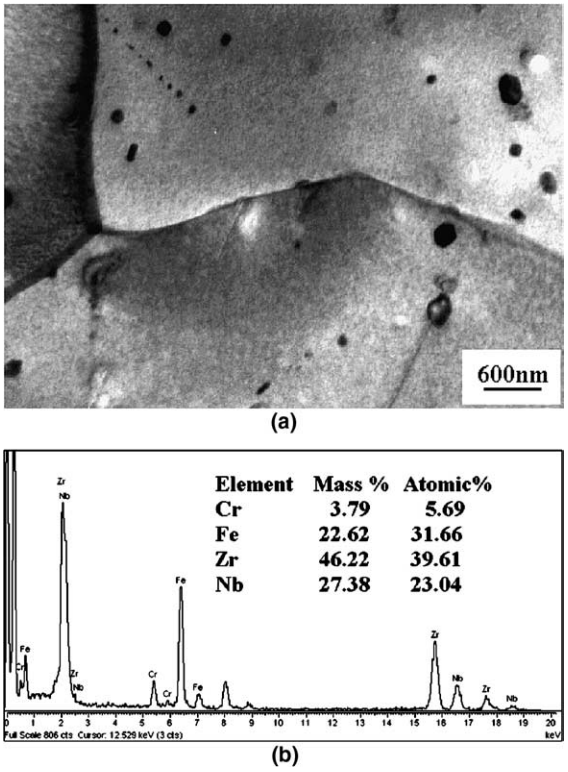

Fig. 4. TEM micrograph and EDS spectrum for precipitates of Zr–Sn–Nb–Fe–Cr specimen treated by 800 °C/560 °C.

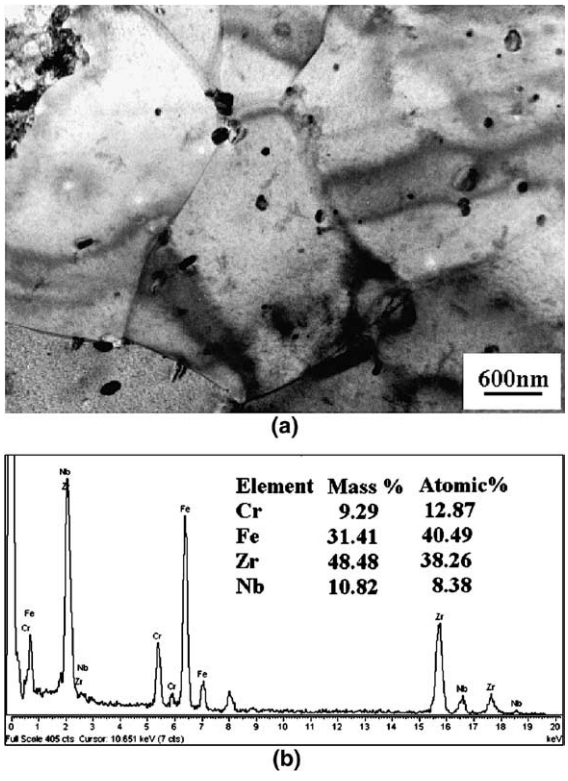

Fig. 5. TEM micrograph and EDS spectrum for precipitates of Zr–Sn–Nb–Fe–Cr specimen treated by 680 °C/500 °C.

Fig. 4(a) shows the precipitates of 800 °C/560 °C specimen. The type, distribution, and shape of precipitates in the specimen were very similar to those in the 800 °C/500 °C specimen, which contained two types of particles. However, in contrast to the 800 °C/500 °C specimen, the composition of Nb in the small precipitate, might be $Zr(Nb,Fe,Cr)_2$, was only 23.04 at.% (Fig. 4(b)). Lower Nb contents in the small precipitate resulted in more Nb dissolved in the matrix, which indicated that the solid solution content of Nb was higher in αZr in 800 °C/560 °C specimen than that in 800 °C/500 °C specimen.

Figs. 5(a) and 6(a) show the precipitates of 680 °C/500°C and 680 °C/560 °C specimens, respectively. Although the distribution, and shape of precipitates in the specimens were very similar to those in the 800 °C/500 °C specimen, only one kind of precipitate, $Zr(Fe,Cr)_2$ type, was identified by EDS (Figs. 5(b) and 6(b)). The Zr–Nb–Fe type precipitate was not observed

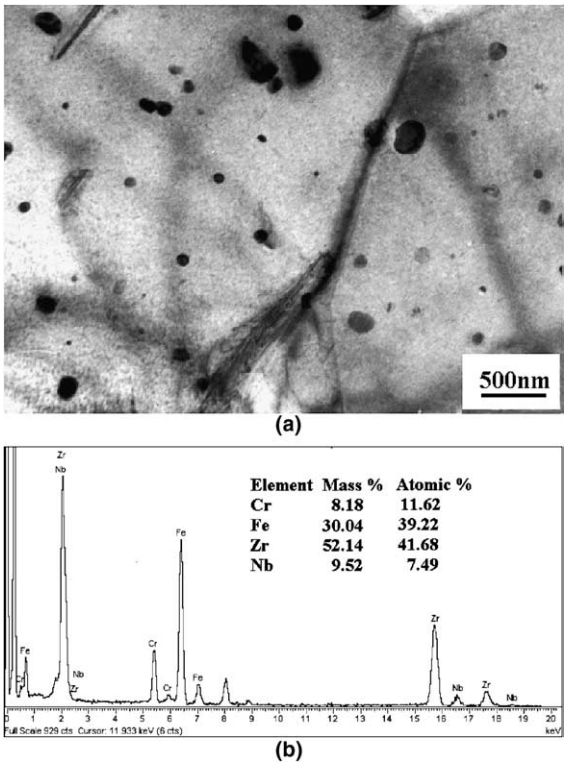

Fig. 6. TEM micrograph and EDS spectrum for precipitates of Zr–Sn–Nb–Fe–Cr specimen treated by 680 °C/560 °C.

in this study. Because Nb content was low in $Zr(Fe,Cr)_2$ type precipitates, much more Nb dissolved in αZr in 680 °C/500 °C and 680 °C/560 °C specimens.

Because the maximum solubility of Fe in αZr is known to be very low(120 ppm at 820 °C [14]) and the Fe content in Zr–Sn–Nb–Fe–Cr alloy used in this study was 0.31 wt%, almost all Fe would be precipitated as $Zr(Fe,Cr)_2$ type and Zr–Nb–Fe type intermetallic precipitates. In the case of 800 °C/500 °C and 800 °C/560 °C specimens, TEM/EDS analyses indicated that there were two types of precipitates and their volume fractions were almost equal. Based on the ratio of Fe/Nb in precipitates analyzed by EDS, the Nb content in precipitates could be calculated. Then the Nb content in αZr, as well as in precipitates could be calculated, which are shown in Table 2. Among these four kinds of specimens, 800 °C/500 °C specimen had the lowest Nb content in αZr due to the formation of Zr–Nb–Fe type precipitate. The results indicated that the formation of Zr–Nb–Fe type precipitate and a low Nb content in αZr was helpful to the corrosion resistance of Zr–Sn–Nb–Fe–Cr zirconium alloy in LiOH aqueous solution.

For better understanding the influence of heat treatment on corrosion resistance and Zr–Sn–Nb–Fe–Cr zirconium alloys, in terms of Zr–Nb binary phase diagram (Fig. 7), the characteristics of microstructure of 800 °C/500 °C specimen in relation to heat treatment can be deduced.

For a binary Zr–Nb alloy containing 0.39 wt% Nb, Fig. 7 shows that αZr matrix containing 0.15 wt% Nb and βZr phase containing much more Nb would be produced by heating to 800 °C in an equilibrium state. When the alloy is annealed at 500 °C after cold rolling, βNb is produced by the decomposition of βZr to αZr + βNb phases. It is easy for βNb phase to precipitate near the defects brought by cold rolling. In the case of 800 °C/500 °C specimen of Zr–Sn–Nb–Fe–Cr alloy, in addition to αZr matrix containing about 0.15 wt% Nb and βZr phase containing much more Nb, there existed stable $Zr(Fe,Cr)_2$ precipitate in the specimens after annealing at 800 °C for an hour. When the specimen was annealed at 500 °C after cold rolling, the stable Zr–Nb–Fe second phase particles were precipitated firstly by the decomposition of βZr. So there were two types of precipitates, $Zr(Fe,Cr)_2$ type and Zr–Nb–Fe type, in the 800 °C/500 °C specimen of Zr–Sn–Nb–Fe–Cr alloy. The formation of stable Zr–Nb–Fe type precipitates resulted in lower Nb content in αZr matrix.

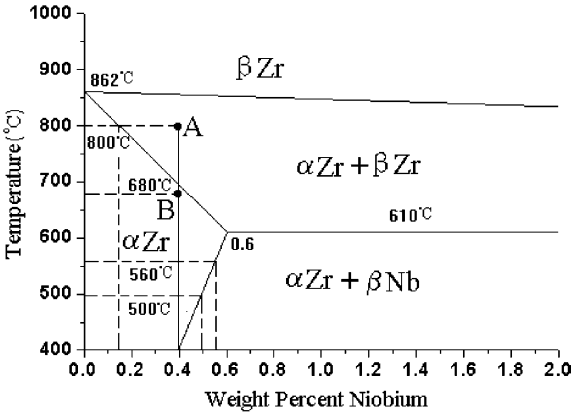

Fig. 7. A part of Zr–Nb phase diagram.

Table 2
Niobium content in αZr solid solution of Zr–Sn–Nb–Fe–Cr alloys with different heat-treatment (wt%)

Heat-treatment	680 °C/500 °C	680 °C/560 °C	800 °C/500 °C	800 °C/560 °C
Type of precipitates	$Zr(Fe,Cr)_2$	$Zr(Fe,Cr)_2$	$Zr(Fe,Cr)_2$ and Zr–Nb–Fe	$Zr(Fe,Cr)_2$ and Zr–Nb–Fe
Fe/Nb in precipitates	About 2.9	About 3.1	About 3.1 and 0.26	About 3.1 and 0.83
Nb-content in αZr	0.33%	0.33%	0.21%	0.29%

For a binary Zr–Nb alloy containing 0.39 wt% Nb, only αZr matrix existed when heated up to 680 °C in an equilibrium state. When the alloy is annealed at 560 °C, no βNb phase precipitates from αZr matrix because the solid solubility of Nb in αZr matrix is about 0.55 wt% at 560 °C. In the case of 680 °C/560 °C specimen of Zr–Sn–Nb–Fe–Cr alloy, it is difficult for Zr–Nb–Fe second phase particles to precipitate, except $Zr(Fe,Cr)_2$ type precipitate existing stable in the specimen early. This results in higher Nb content in αZr matrix. The analyses results show that the 800 °C/500 °C specimen in this study contains less Nb in αZr matrix than the 680 °C/560 °C specimen, which is consistent with the calculation results based on the EDS analyses shown in Table 2.

4. Conclusion

The corrosion behavior of Zr–Sn–Nb–Fe–Cr zirconium alloy was observed to have no certain relation to the accumulated annealing parameter.

On the basis of the EDS study and phase diagram analyses, it is suggested that the intermediate annealing at 800 °C before the final cold rolling reduced Nb content in αZr matrix and produced Zr–Nb–Fe precipitates after aging at 500 °C, which results in an improvement in the corrosion resistance of Zr–Sn–Nb–Fe–Cr zirconium alloy.

Acknowledgment

The authors are grateful to the financial support of the National Natural Science Foundation of China (Grant no. 50301009), the Education Development Foundation of Shanghai (Grant no. 03AK24) and Shanghai Natural Science Foundation (Grant no. 04ZR14057).

References

[1] R.J. Comstock, G. Schoenberger, G.P. Sable, Zirconium in the Nuclear Industry, Eleventh International Symposium, ASTM STP 1295, America Society for Testing and Materials, Philadelphia, PA, 1996, p. 710.
[2] J.P. Mardon, D. Charquet, J. Senevat, Zirconium in the Nuclear Industry, Twelfth International Symposium, ASTM STP 1354, America Society for Testing and Materials, West Conshohocken, PA, 2000, p. 505.
[3] A.V. Nikulina, V.A. Markelov, M.M. Peregud, Y.K. Bibilashvili, V.A. Kotrekhow, A.F. Lositsky, N.V. Kuzmenko, Y.P. Shevnin, V.K. Shamardin, G.P. Kobylyansky, A.E. Novoselov, Zirconium in the Nuclear Industry, Eleventh International Symposium, ASTM STP 1295, America Society for Testing and Materials, Philadelphia, PA, 1996, 1996, p. 785.
[4] W.J. Zhao, Z. Miao, H.M. Jiang, X.W. Yu, W.J. Li, C. Li, B.X. Zhou (in Chinese), J. Chin. Soc. Corros. Prot. 22 (2) (2002) 124.
[5] T. Thorvaldsson, T. Andersson, A. Wilson, A. Wardle, Zirconium in the Nuclear Industry, Eighth International Symposium, ASTM STP 1023, America Society for Testing and Materials, Philadelphia, PA, 1989, p. 128.
[6] F. Garzarolli, E. Steinberg, H.G. Weidinger, Zirconium in the Nuclear Industry, Eighth International Symposium, ASTM STP 1023, America Society for Testing and Materials, Philadelphia, PA, 1989, p. 202.
[7] P. Rudling, H. Pettersson, T. Andersson, T. Thorvaldsson, Zirconium in the Nuclear Industry, Eighth International Symposium, ASTM STP 1023, America Society for Testing and Materials, Philadelphia, PA, 1989, p. 213.
[8] B.X. Zhou, W.J. Zhao, Z. Miao, S.F. Pan, C. Li, Y.R. Jiang, China Nuclear Science and Technology Report, CNIC-01074, SINRE-0066, China Nuclear Information Center, Atomic Energy Press, 1996.
[9] J.H. Baek, Y.H. Jeong, I.S. Kim, J. Nucl. Mater. 280 (2000) 235.
[10] T. Isobe, Y. Matsuo, Zirconium in the Nuclear Industry, Ninth International Symposium, ASTM STP 1132, America Society for Testing and Materials, Philadelphia, PA, 1991, p. 346.
[11] Q. Li, W.Q. Liu, B.X. Zhou (in Chinese), Rare Metal Mater. Eng. 31 (5) (2002) 389.
[12] W.Q. Liu, Q. Li, B.X. Zhou, M.Y. Yao (in Chinese), Nucl. Power Eng. 24 (1) (2003) 33.
[13] Y.S. Kim, S.K. Kim, J.G. Bang, Y.H. Jung, J. Nucl. Mater. 279 (2000) 335.
[14] D. Charquet, R. Hahn, E. Ortlieb, J.P. Gros, J.F. Wadier, Zirconium in the Nuclear Industry, Eighth International Symposium, ASTM STP 1023, America Society for Testing and Materials, Philadelphia, PA, 1989, p. 405.